13th World Conference on Earthquake Engineering
Vancouver, B.C., Canada
August 1-6, 2004
Paper No. 2229

SPREAD–OF–PLASTICITY ANALYSIS OF R/C BUILDINGS, SUBJECTED TO MONOTONIC 'SEISMIC' LOADING

Petros MARATHIAS[1], Evangelos VISVIKIS[2], Panagiotis MOUSOULEAS[3] and Vassilis YANNOPOULOS[4]

SUMMARY

A commonly used philosophy for the design of building structures is based on ductility, as the design of non seismic–isolated structures that remain elastic during severe earthquakes is extremely expensive. The ductile design aims to minimize the potential damage and life loss mainly by preventing the collapse of the structure. This is achieved if the structure is capable of sustaining considerable inelastic deformations without increase of its internal forces beyond an ultimate limit and without leading to instability. In the present research work, a non–linear analysis program has been developed for the calculation of total ductility of reinforced concrete space frame buildings. A new spread–of–plasticity model is introduced for the idealization of reinforced concrete members of arbitrarily shaped cross–sections, subjected to biaxial bending and axial forces. Gradual yielding of the cross–sections' fibbers is taken into account through analytical integration over the cross–sections' area. Two R/C structures subjected to monotonic loading, which is applied incrementally until collapse, are analyzed and their global ductility capacity is estimated. Furthermore, local ductility capacities, expressed in terms of lateral load–strain curves of specific steel bars, are also presented for these structures.

INTRODUCTION

The most common earthquake–resistant design philosophy employed worldwide nowadays is the one based on the concept of ductility. The objective of modern design codes is to produce structures that have high levels of ductility, so that when the design earthquake occurs, the structures will remain stable and whole, preventing the loss of life. This goal is achieved by the formation of the proper elastoplastic mechanism during the design earthquake. This mechanism must reliably ensure that the structure is capable of undergoing large horizontal displacements (δ), without collapse, through the inelastic deformations in prescribed areas. In these areas (e.g. the ends of the beams and the bases of the columns) the construction materials are stressed beyond their elastic range of behavior.

The elastoplastic mechanism mentioned above, is idealized and analyzed until collapse for the design earthquake load pattern, in order to estimate (a) the strength and deformation capacities of various elements, and (b) the ductility capacity of the whole structure.

[1]Dr., Lecturer, Dep. of Civil Eng., University of Patras, Greece, email: marathias@statik.civil.upatras.gr
[2]Post–graduate, Dep. of Civil Eng., University of Patras, Greece
[3]Post–graduate, Dep. of Civil Eng., University of Patras, Greece
[4]Civil Engineer, Greece

The analysis of the elastoplastic mechanism can be performed with the non–linear dynamic analysis, which is the most sophisticated analytical tool currently available for this purpose. However, this kind of analysis requires extensive resources in computation, as well as for the interpretation of the results. For this reason, it is common in practice to use the non–linear static analysis of the elastoplastic mechanism with an equivalent static load pattern. This kind of analysis demands an as accurate as possible idealization of the areas where plastic deformations are likely to occur. When these areas are small in length this idealization can be performed with the introduction of a local elastoplastic hinge. The procedures where such idealizations take place are called discrete model procedures. On the other hand, if the areas where plastic deformations occur are spread at a distance, even as large as the element's length, then the above–mentioned idealization is unacceptable. The procedures, where the true distribution of deformations is taken into account, are called spread–of–plasticity model procedures.

The discrete model

The discrete model is the most commonly used model in the non–linear analysis procedures whose aim is the analysis of the elastoplastic mechanism of structures and it can be found in most widely used civil engineering software packages [1], [2]. A simple approach to the calculation of the structure's response is with the sequential application of linear analysis software. As the loading increases, a change in stiffness properties of the elements is achieved by placing a local hinge, whenever the flexural yielding strength of a cross–section has been reached. The internal forces and deformations from all previous loading stages are added up to reflect the analysis results. Thus, a substantial amount of manual bookkeeping is required while the results obtained by these successive linear analyses are inherently approximate and weak in assessment of the true member forces. Despite these facts, this method can provide a good approximation to the elastoplastic mechanism of the structure. A more sophisticated approach is the formulation of a beam/column element and a lot of research has been conducted in this field. There are element formulations that use uncoupled moment/torsion–rotation and shear/axial force–displacement diagrams [1] in order to represent the cross–section's behavior under gradually increased levels of loading. Other elements have the capability to model flexural yielding, plastic axial deformation and changes in axial stiffness [3].

The spread–of–plasticity model

The spread–of–plasticity model provides more in depth analysis and superior accuracy in the results than the discrete model, as it takes into account the fact that yielding does not occur in an infinitesimal length of a beam/column element but instead, it is spread in a finite area. Many beam/column elements have also been developed in this field of research and some of them have already been implemented in software packages. The ANSYS program [4] has beam/column elements that use linear and quadratic shape functions for the displacement along the element's length, and it can integrate the stresses over a large number of cross–sectional shapes. The ADINA program [5] utilizes Hermitian polynomial shape functions, but it can integrate stresses on rectangular and circular cross–sections only. However, ADINA has the capability of calculating the stress resultants, along the element's length, from uncoupled moment/torsion–rotation and shear/axial force–displacement diagrams. Some researchers utilize more complex procedures. Davenne et al. [6] developed an element that employs the standard Hermitian polynomial shape functions to describe the variation of the displacement field along the beam/column. The difference with the 'classical' beam/column elements [7] is that both E and G of the materials vary over the area of the cross–section. Izzudin et al. [8] present a beam/column formulation with quartic shape functions to represent the two transverse displacements and use a constant axial force criterion instead of shape functions for the axial displacement.

In the present study a non–linear static analysis procedure that incorporates R/C material is developed and a new spread–of–plasticity beam/column element is introduced for this purpose. After the comprehensive presentation, the procedure is applied to a multi–storey moment resisting frame and a cantilever shear wall. The results of these analyses are plotted in diagrams and discussed.

PROPOSED ANALYSIS PROCEDURE

This section describes the procedure for the calculation of ductility capacity of reinforced concrete space frame buildings. A new spread–of–plasticity element is introduced for the idealization of R/C members of arbitrarily shaped cross–section. The procedure consists of three interconnected phases:

1. Pushover analysis.
2. Formulation of the spread–of–plasticity element.
3. Calculation of cross–section's strains.

The following assumptions are made:

1. The elements are based on Timoshenko's beam theory, which is a first order shear deformation theory: transverse shear strain is constant through the cross–section; that is, cross–sections remain plane and undistorted after deformation.
2. The elements use a linear elastic relationship between shearing forces–transverse displacements and torsional moment–twist angle.
3. Concrete is consistent with conventional R/C cross–section design, where only the steel reinforcement provides tensile resistance.

Pushover analysis

Pushover analysis is an automated non–linear incremental load analysis, which contains a procedure that automatically searches for the load level (λ), at which structural instability or collapse occurs. The external loading imposed on the structure is calculated from the following equation:

$$\{P\} = \{P_{con}\} + \lambda \cdot \{P_{inc}\} \tag{1}$$

where $\{P_{con}\}$ and $\{P_{inc}\}$ are the pushover analysis' constant and incremental loading conditions, respectively. The steps of the pushover analysis are described below and illustrated in Figure 1 (the subscript (k) represents the kth load step):

1. Given the load level (λ), form the external load vector $\{P\}_k$, using equation (1).
2. Calculate nodal displacements $\{u\}_k$ for the given $\{P\}_k$ by solving the non–linear system of equations:

   $$\{u\}_k = [K(u)]_k^{-1} \cdot \{P\}_k \tag{2}$$

   These are solved by implementing the Newton–Raphson iterative method [9].
3. If the Newton–Raphson procedure has successfully converged, then checking of materials' deformations is performed. The materials of the structure are checked against the ultimate deformation level, which is defined by their stress–strain diagrams. If a material fracture is detected, at any point in the structure, the current load increment ($\Delta\lambda$) is decreased, a new load level (λ) is calculated and the procedure resumes from the first step.
   Otherwise, the current load level (λ) and the displacements $\{u\}_k$ corresponding to $\{P\}_k$ are stored, a new load increment ($\Delta\lambda$) is added to the current load level and the procedure resumes from the first step. If the maximum permissible number of load increment's reductions is exceeded, or the load increment becomes less than a minimum value the pushover analysis is terminated.

At each iteration of the Newton–Raphson procedure, the spread–of–plasticity elements must calculate their internal forces $\{\Phi\}$ and their tangent stiffness matrix $[K_t]$. These issues will be addressed in the next section.

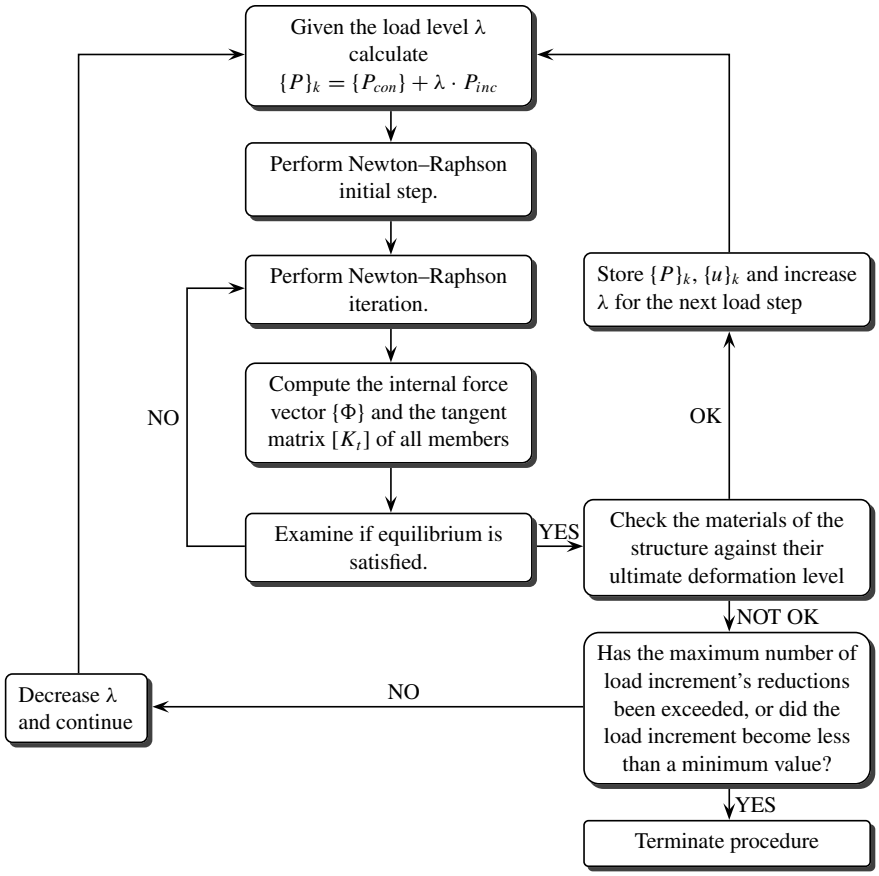

Figure 1: The pushover analysis procedure.

Formulation of the spread–of–plasticity element

The spread–of–plasticity beam/column element proposed in this research work, is presented in Figure 2.

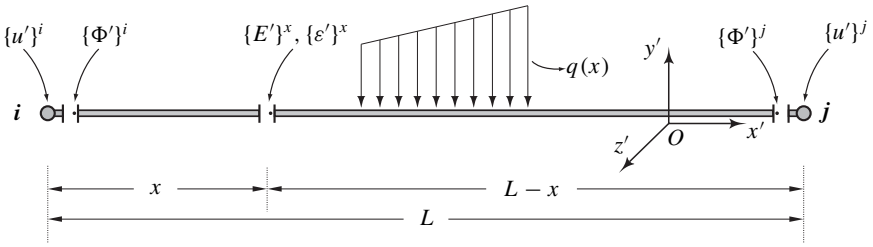

Figure 2: Spread–of–plasticity element.

More specifically, the derivation of the internal force vector $\{\Phi\}$ and the formation of the tangent stiffness matrix $[K_t]$ of the element are discussed.

Calculation of internal forces $\{\Phi\}$

The internal force vector $\{\Phi\}$ of the element is calculated by an iterative procedure. The steps of this calculation are listed below and illustrated in Figure 3 (the subscript (m) indicates the mth iteration):

1. Transform the global displacements $\{u\}^i$, $\{u\}^j$ of the end nodes to the element's coordinate system $\{u'\}^i$, $\{u'\}^j$ and apply the externally imposed loads $q(x)$ along the element's length.

2. Estimate the initial internal forces $\{\Phi'\}$ in the element's coordinate system, using elastic assumptions for the element.

3. Obtain the stress resultants $\{E'\}_m^x$ of a cross–section at distance x from the start node of the element, by applying the equilibrium equations. Gauss numerical integration scheme dictates the number of cross–sections where the stress resultants $\{E'\}_m^x$ are calculated.

4. Calculate the strains $\{\varepsilon'\}_m^x$ for each of the above cross–sections. This issue will be discussed in the next section.

5. The displacements of the end node of the element $\{u'\}_m^j$ are calculated with the use of the virtual work principle [10] (integrating $\{\varepsilon'\}_m^x$ along the element's length) and by adding the element's rigid body motion due to the displacements $\{u'\}^i$. Specifically,

$$
\begin{aligned}
u^j_{x'} &= \int_0^L \varepsilon_{x'}(x)\cdot(-1)dx + u^i_{x'} \\
u^j_{y'} &= \int_0^L \gamma_{x'y'}(x)\cdot(-1)dx - \int_0^L \phi_{z'}(x)(L-x)dx + u^i_{y'} + \vartheta^i_{z'}\cdot L \\
u^j_{z'} &= \int_0^L \gamma_{x'z'}(x)\cdot(-1)dx + \int_0^L \phi_{y'}(x)(L-x)dx + u^i_{z'} - \vartheta^i_{y'}\cdot L \\
\vartheta^j_{x'} &= \int_0^L \phi_{x'}(x)\cdot(-1)dx + \vartheta^i_{x'} \\
\vartheta^j_{y'} &= \int_0^L \phi_{y'}(x)\cdot(-1)dx + \vartheta^i_{y'} \\
\vartheta^j_{z'} &= \int_0^L \phi_{z'}(x)\cdot(-1)dx + \vartheta^i_{z'}
\end{aligned}
\tag{3}
$$

Equations (3) can be written in a matrix form:

$$
\begin{bmatrix} u^j_{x'} \\ u^j_{y'} \\ u^j_{z'} \\ \vartheta^j_{x'} \\ \vartheta^j_{y'} \\ \vartheta^j_{z'} \end{bmatrix}
= -\int_0^L \begin{bmatrix} 1 & 0 & 0 & 0 & 0 & 0 \\ 0 & 1 & 0 & 0 & 0 & (L-x) \\ 0 & 0 & 1 & 0 & -(L-x) & 0 \\ 0 & 0 & 0 & 1 & 0 & 0 \\ 0 & 0 & 0 & 0 & 1 & 0 \\ 0 & 0 & 0 & 0 & 0 & 1 \end{bmatrix} \cdot \begin{bmatrix} \varepsilon_{x'}(x) \\ \gamma_{x'y'}(x) \\ \gamma_{x'z'}(x) \\ \phi_{x'}(x) \\ \phi_{y'}(x) \\ \phi_{z'}(x) \end{bmatrix} dx + \begin{bmatrix} u^i_{x'} \\ u^i_{y'} + \vartheta^i_{z'}\cdot L \\ u^i_{z'} - \vartheta^i_{y'}\cdot L \\ \vartheta^i_{x'} \\ \vartheta^i_{y'} \\ \vartheta^i_{z'} \end{bmatrix}
\tag{4}
$$

or more conveniently:

$$
\{u'\}^j_m = -\int_0^L [F]\cdot\{\varepsilon'\}^x_m dx + \{T\}
\tag{5}
$$

It should be noted that equations (3) are valid under the assumption of small nodal rotations in the element's coordinate system. The integrals of equations (5) are calculated numerically using Gauss integration scheme.

6. Form a new tangent stiffness matrix $[K_t]_m$ for the element, as described in the next paragraph.

7. Examine if displacements $\{u'\}_m^j$ are equal to the initially imposed $\{u'\}^j$:

   a) If this condition is satisfied, then the internal forces $\{\Phi'\}_m^j$ are compatible with $\{u'\}^j$. Applying equilibrium equations for the whole element provides the internal forces $\{\Phi'\}_m^i$ and the procedure is terminated by calculating the internal force vector $\{\Phi\}$ in the global coordinate system.

   b) If this condition is not satisfied, a new vector $\{\Phi'\}_{m+1}^j$ is calculated, using:

$$\{\Phi'\}_{m+1}^j = \{\Phi'\}_m^j + [K_t^{jj}]_m \cdot (\{u'\}^j - \{u'\}_m^j) \tag{6}$$

   where $[K_t^{jj}]$ is a submatrix of the element's stiffness matrix $[K_t]_m$ and the procedure resumes from step 3.

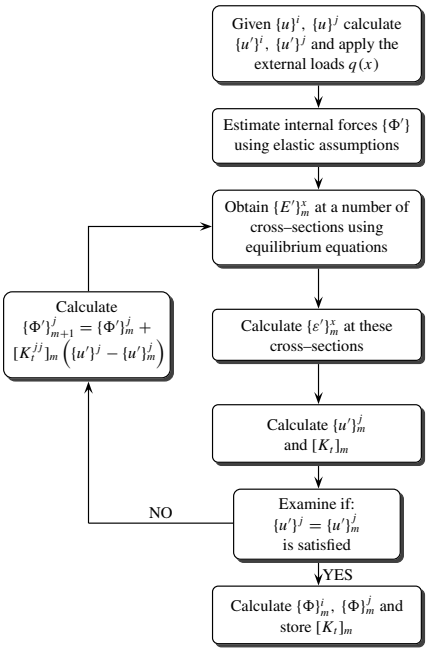

Figure 3: Calculation of internal forces $\{\Phi\}$ and tangent stiffness matrix $[K_t]$ of the element.

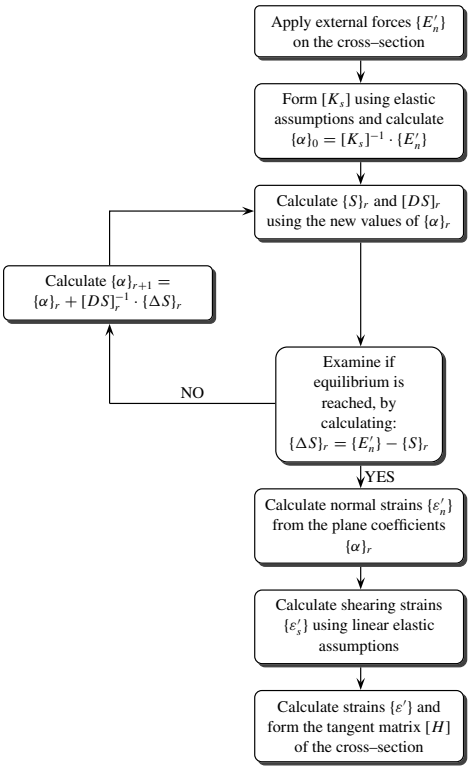

Figure 4: Calculation of the cross–section's strains.

Formation of the tangent stiffness matrix $[K_t]_m$

An infinitesimal variation of nodal forces $\{d\Phi'\}_m^j$ results, after applying equilibrium equations, in the following variation of internal forces $\{dE'\}_m^x$, at a random cross–section:

$$\{dE'\}_m^x = -\begin{bmatrix} 1 & 0 & 0 & 0 & 0 & 0 \\ 0 & 1 & 0 & 0 & 0 & 0 \\ 0 & 0 & 1 & 0 & 0 & 0 \\ 0 & 0 & 0 & 1 & 0 & 0 \\ 0 & 0 & -(L-x) & 0 & 1 & 0 \\ 0 & (L-x) & 0 & 0 & 0 & 1 \end{bmatrix} \cdot \{d\Phi'\}_m^j \quad \text{or} \quad \{dE'\}_m^x = -[G] \cdot \{d\Phi'\}_m^j \tag{7}$$

As it will be discussed in the next section, for each combination of imposed stresses on the cross–section, a relation reflecting the infinitesimal variation of the cross–section's stress resultants $\{dE'\}_m^x$ with the strains $\{d\varepsilon'\}_m^x$ can be obtained:

$$\{dE'\}_m^x = [H]_m \cdot \{d\varepsilon'\}_m^x \tag{8}$$

where $[H]_m$ is the tangent matrix of the cross–section. By solving this equation for $\{d\varepsilon'\}_m^x$ we obtain:

$$\{d\varepsilon'\}_m^x = [H]_m^{-1} \cdot \{dE'\}_m^x \tag{9}$$

Substitution of equation (7) into equation (9) gives:

$$\{d\varepsilon'\}_m^x = -[H]_m^{-1} \cdot [G] \cdot \{d\Phi'\}_m^j \tag{10}$$

Using equation (5), the infinitesimal variation of deformation functions along the element length $\{d\varepsilon'\}_m^x$ is related to the corresponding variation of displacements $\{du'\}_m^j$ as shown below:

$$\{du'\}_m^j = -\int_0^L [F] \cdot \{d\varepsilon'\}_m^x dx \tag{11}$$

Substituting equation (10) in equation (11) results in:

$$\{du'\}_m^j = \left(\int_0^L [F] \cdot [H]_m^{-1} \cdot [G] dx\right) \cdot \{d\Phi'\}_m^j \quad \text{or} \quad \{du'\}_m^j = [K_t^{jj}]_m^{-1} \cdot \{d\Phi'\}_m^j \tag{12}$$

The integrals of the above equation represent the inverted stiffness matrix $[K_t^{jj}]_m$ of the element, which relates the variation of nodal displacements $\{du'\}_m^j$ to the variation of nodal forces $\{d\Phi'\}_m^j$. These integrals are calculated using Gauss integration scheme. The tangent stiffness matrix $[K_t]_m$ of the element is then easily derived.

Calculation of cross–section's strains

The calculation of strains $\{\varepsilon'\}$ on an arbitrarily shaped R/C cross–section, is presented here. The shape of the R/C cross–section, the positions and diameters of steel bars, the non–linear stress–strain diagrams for concrete and steel material and the external for the cross–section normal stress resultants $\{E_n'\} = \begin{bmatrix} R_{x'} & M_{z'} & M_{y'} \end{bmatrix}^T$ originating from $\{E'\}^x$, are needed for the calculation of the strains. The strains of any point $P(y', z')$ on the cross–section are calculated by evaluating the equation of the strain plane (see Figure 5), which is defined when equilibrium in the cross–section has been achieved, that is:

$$\{S\} = \{E_n'\} \tag{13}$$

where $\{S\} = \begin{bmatrix} R_{x'} & M_{z'} & M_{y'} \end{bmatrix}^T$ is the cross–section's normal stress resultants vector. The equation of such a plane is:

$$\varepsilon(y', z') = \alpha_1 + \alpha_2 \cdot y' + \alpha_3 \cdot z' \tag{14}$$

where y', z' are the coordinates of a point on the cross–section, and $\alpha_1, \alpha_2, \alpha_3$ are the plane coefficients, as illustrated in Figure 5. It is evident that if point O coincides with the centroid of the cross–section, then α_1, α_2 and α_3 will express the strains $\{\varepsilon_n'\}$ of the cross–section, due to normal stresses:

$$\{\varepsilon_n'\} = \begin{bmatrix} \varepsilon_{x'} & \phi_{y'} & \phi_{z'} \end{bmatrix}^T = \begin{bmatrix} \alpha_1 & \alpha_3 & -\alpha_2 \end{bmatrix}^T \tag{15}$$

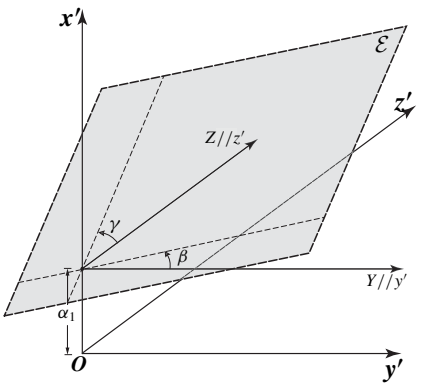

α_1 = distance of the plane's intersection point with the vertical axis x', from O.
$\alpha_2 = \tan\hat{\beta}$ (slope of the plane with respect to the y'axis.)
$\alpha_3 = \tan\hat{\gamma}$ (slope of the plane with respect to the z'axis.)

Figure 5: The strain plane.

The cross–section's normal stress resultants $\{S\}$ are calculated from the following integrals :

$$R_{x'} = \int_A \sigma(\varepsilon) dA, \quad M_{z'} = \int_A \sigma(\varepsilon) \cdot y' dA, \quad M_{y'} = \int_A \sigma(\varepsilon) \cdot z' dA \tag{16}$$

where A is the area of the cross–section and $\sigma(\varepsilon)$ the normal stresses over the area. Relations (16) form a system of equations that relates the cross–section's normal stress resultants $\{S\}$ to the plane coefficients $\{\alpha\}$:

$$\{S\} = [K_s(\alpha)] \cdot \{\alpha\}, \quad \text{where} \quad \{\alpha\} = \begin{bmatrix} \alpha_1 & \alpha_2 & \alpha_3 \end{bmatrix}^T \tag{17}$$

and matrix $[K_s(\alpha)]$ is depending on the geometric properties of the cracked cross–section and the materials' stress–strain relationships. This is a non–linear system of equations, which can be solved by utilizing the Newton–Raphson method. The steps of this procedure are listed below and illustrated in Figure 4 (the subscript (r) indicates the rth iteration):

1. Apply the stress resultants $\{E'_n\}$ as external loads on the geometric center of the cross–section.

2. Form matrix $[K_s]$ based on the uncracked cross–section consisting of elastic materials, and compute the initial plane coefficients as:

$$\{\alpha\}_0 = [K_s]^{-1} \cdot \{E'_n\} \tag{18}$$

3. Calculate cross–section's stress resultants $\{S\}_r$ by equation (16).

4. Examine if equilibrium condition for the cross–section is satisfied, by calculating:

$$\{\Delta S\}_r = \{E'_n\} - \{S\}_r \tag{19}$$

   If equilibrium is valid, then this procedure is terminated and the normal strains $\{\varepsilon'_n\}$ are calculated from the strain plane coefficients $\{\alpha\}_r$, using equation (15).

   If equilibrium is unsatisfied then continue with the next step.

5. Compute new plane coefficients from the following equations:

$$\{\alpha\}_{r+1} = \{\alpha\}_r + [DS]_r^{-1}\{\Delta S\}_r \tag{20}$$

where as $[DS]_r$ any matrix that relates the variation of stress resultants $\{\Delta S\}_r$ to the variation of the plane coefficients $\{\Delta\alpha\}_r = \{\alpha\}_{r+1} - \{\alpha\}_r$, can be used. A tangent matrix $[DS]_r$ has been introduced by Konrad [11] as:

$$[DS]_r = \begin{bmatrix} \frac{\partial R_{x'}}{\partial \alpha_1} & \frac{\partial R_{x'}}{\partial \alpha_2} & \frac{\partial R_{x'}}{\partial \alpha_3} \\ \frac{\partial M_{z'}}{\partial \alpha_1} & \frac{\partial M_{z'}}{\partial \alpha_2} & \frac{\partial M_{z'}}{\partial \alpha_3} \\ \frac{\partial M_{y'}}{\partial \alpha_1} & \frac{\partial M_{y'}}{\partial \alpha_2} & \frac{\partial M_{y'}}{\partial \alpha_3} \end{bmatrix}_r \tag{21}$$

6. The procedure resumes from step 3.

For the calculation of the cross–section's strains due to shearing stresses $\{\varepsilon'_s\}$, the assumption of linear elastic stress–strain relationship has been made. The cross–section's shearing strains $\{\varepsilon'_s\}$ are calculated by:

$$\{\varepsilon'_s\} = \begin{bmatrix} \gamma_{x'y'} & \gamma_{x'z'} & \phi_{x'} \end{bmatrix}^T = \begin{bmatrix} \frac{R_{y'}}{GA_{y'}} & \frac{R_{z'}}{GA_{z'}} & \frac{M_{x'}}{GI_{x'}} \end{bmatrix}^T \tag{22}$$

where G is the elastic shear modulus, $A_{y'}$ and $A_{z'}$ the shear areas of the uncracked cross–section with respect to y' and z' axes of the element, respectively and $I_{x'}$ is its torsion moment of inertia.
It becomes obvious that the strains $\{\varepsilon'\}$ can be deduced from the normal $\{\varepsilon'_n\}$ and the shearing $\{\varepsilon'_s\}$ strains. The tangent matrix $[H]$ of the cross–section can be calculated from the following:

$$[H] = \begin{bmatrix} \frac{\partial R_{x'}}{\partial \alpha_1} & 0.0 & 0.0 & 0.0 & \frac{\partial R_{x'}}{\partial \alpha_3} & \frac{\partial R_{x'}}{\partial \alpha_2} \\ 0.0 & G \cdot A_{y'} & 0.0 & 0.0 & 0.0 & 0.0 \\ 0.0 & 0.0 & G \cdot A_{z'} & 0.0 & 0.0 & 0.0 \\ 0.0 & 0.0 & 0.0 & G \cdot I_{x'} & 0.0 & 0.0 \\ \frac{\partial M_{y'}}{\partial \alpha_1} & 0.0 & 0.0 & 0.0 & \frac{\partial M_{y'}}{\partial \alpha_3} & \frac{\partial M_{y'}}{\partial \alpha_2} \\ \frac{\partial M_{z'}}{\partial \alpha_1} & 0.0 & 0.0 & 0.0 & \frac{\partial M_{z'}}{\partial \alpha_3} & \frac{\partial M_{z'}}{\partial \alpha_2} \end{bmatrix} \tag{23}$$

NUMERICAL STUDIES

The proposed analysis method is implemented in the case of an eight–storey R/C frame of an existing building and on a cantilever shear wall, which is part of the earthquake resisting elements of another multi–storey R/C building. These examples have been chosen as representatives of two common structural systems: the moment resisting frame system and the shear wall system.

Multi–storey R/C frame

The configuration and geometry of the eight–storey R/C frame are illustrated in Figure 6. The frame is fully supported and is subjected to uniform gravity loads on its beams. The vertical distribution of lateral inertia loads corresponding to the design earthquake is also illustrated. Spread–of–plasticity elements are used to

model the ground storey columns and the internal beams at all levels. The rest of the members are idealized as elastic elements. This approach was adopted, because base–support sections of ground storey columns and both end–sections of internal beams are potential plastic regions. The dimensions and reinforcement for both spread–of–plasticity and elastic beams are shown in table 1 of Figure 6. Different longitudinal reinforcement at the two end–sections is taken into account using two discrete segments. Each of these segments extends at length equal to half the beam's length and is represented by a different cross–section. Similarly, table 2 summarizes the corresponding data for the columns. The spread–of–plasticity columns are discretized in three segments of 2.0m, 1.0m and 1.45m in length, respectively. The steel reinforcement of ground storey columns is assumed uniformly distributed around the perimeter. On the other hand, the steel reinforcement of internal beams is given with respect to both the upper and lower faces of the cross–section. The cover of reinforcement bars is 35mm.

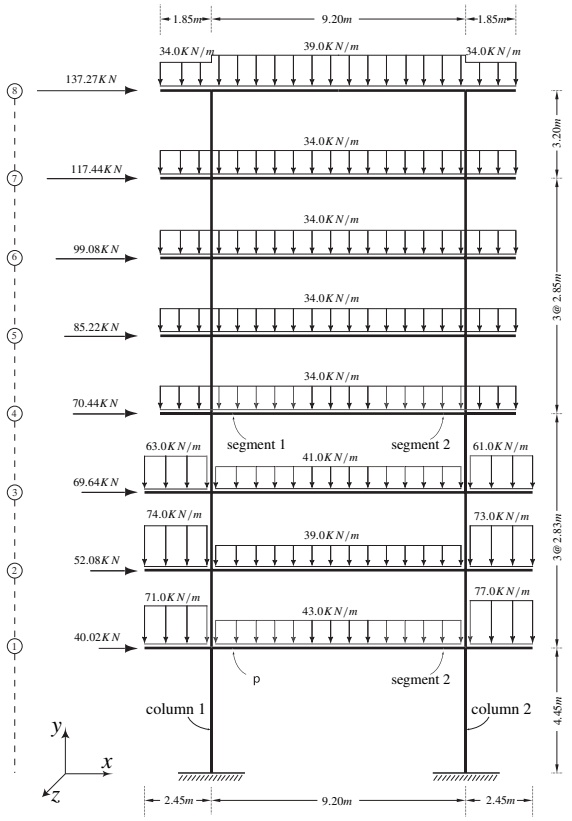

Table 1: Dimensions and reinforcement for beams

Level	Segment	Dimensions (cm	cm)	Longitudinal reinforcement		Transverse reinforcement
				Upper face	Lower face	
Internal beams						
1	1	90	50	15 Φ20	16 Φ16	Φ10/10
1	2	90	50	10 Φ25	16 Φ16	Φ10/10
2	-	90	50	11 Φ25	10 Φ20	Φ8/10
3	-	90	50	11 Φ25	7 Φ25	Φ8/10
4	1	90	50	19 Φ18	10 Φ20	Φ8/10
4	2	90	50	10 Φ25	10 Φ20	Φ8/10
5	-	90	50	15 Φ20	10 Φ20	Φ8/10
6	-	90	50	11 Φ22	6 Φ25	Φ8/10
7	-	90	50	8 Φ25	7 Φ20	Φ8/10
8	-	90	50	14 Φ18	5 Φ22	Φ8/10
Cantilever beams						
1, 4-8	-	90	30	-	-	-
2, 3	-	130	30	-	-	-

Table 2: Dimensions and reinforcement for columns

Level	Segment	Dimensions (cm	cm)	Longitudinal reinforcement	Transverse reinforcement
1	1	110	70	52 Φ25	Φ12/10
1	2	110	70	52 Φ25	Φ8/10
1	3	110	70	32 Φ25	Φ8/10
2	-	110	70	-	-
3-5	-	100	70	-	-
6-8	-	90	70	-	-

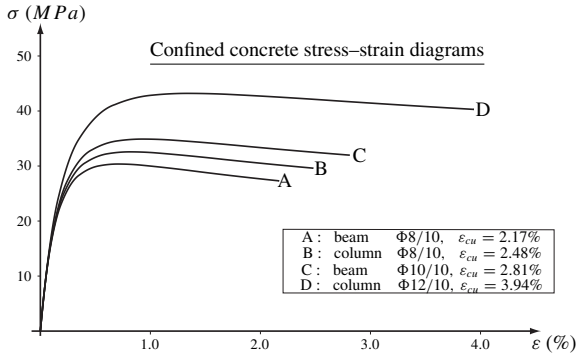

Figure 6: Eight–storey R/C moment resisting frame.

The material properties used for the elastic members are: $E = 2.9 \cdot 10^7 KN/m^2, G = 1.208 \cdot 10^7 KN/m^2$. For the spread–of–plasticity elements, bilinear and non–linear stress–strain relations were assumed for reinforcing steel (S500) and concrete (C20/25), respectively. More specifically, for reinforcing steel a bilinear relation was adopted having the following characteristics: Modulus of elasticity 210GPa, yielding strength 500MPa, ultimate strength 525MPa and ultimate strain 5%. As for concrete, confinement was taken into consideration by utilizing Mander's [12] stress–strain model as shown in Figure 6. Four different categories of confined concrete were modeled according to the volumetric ratio of transverse reinforcement of the cross–sections. In the same figure, the ultimate compressive strain for each of the above concrete materials is given.

The lateral load–top displacement curve, obtained using the proposed analysis method, is presented in Figure 7 together with its bilinear approximation. Lateral loads are expressed in terms of percentage (%) of the design earthquake corresponding to this building. The ductility capacity [9] of the frame is estimated as the ratio :

$$\mu = \frac{\delta_{max}}{\delta_y} = \frac{1.01}{0.3} = 3.37$$

where δ_{max} and δ_y are the maximum and yield lateral displacements of the frame. These two values can be directly obtained from Figure 7.

The ϕ_z rotation diagrams for various load steps of both columns, are also illustrated in Figure 7. Given those diagrams and the geometry configuration of the columns' sections, the strains over the length of the columns for all steel bars can be calculated.

The lateral load–strain relations for the steel bars with the highest tensile strain at the base of the two ground storey columns are shown in Figure 8. Note that at the end of the analysis, the steel bar of column 1 reaches its ultimate tensile strain (5%) and thus causes the termination of the analysis procedure.

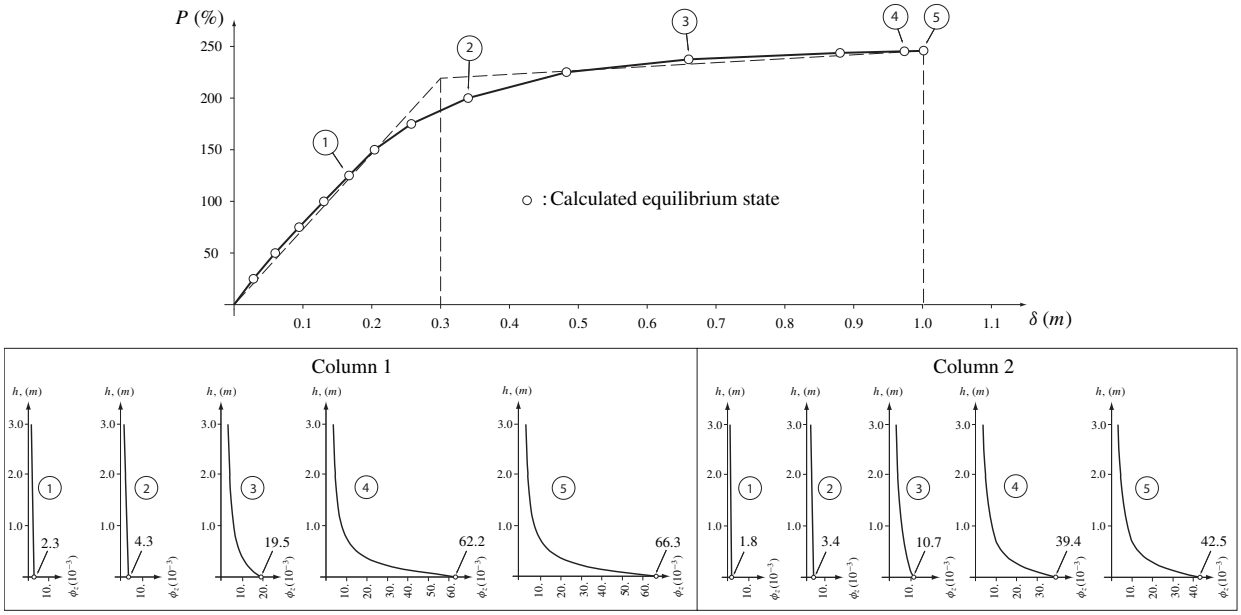

Figure 7: Lateral load–top displacement curve of R/C frame and ϕ_z diagrams (in rad) of columns 1, 2.

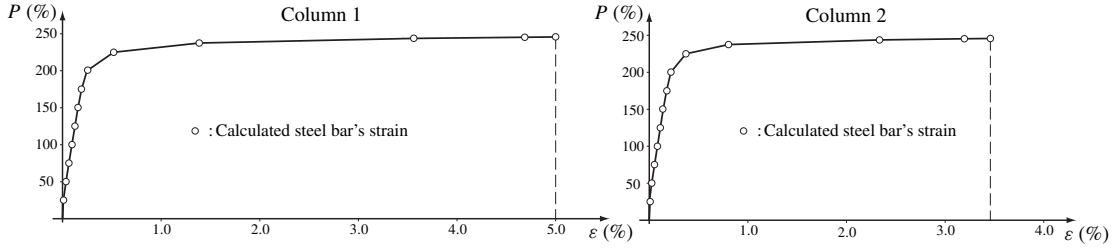

Figure 8: Lateral load–strain curves for the most tensiled steel bars at columns 1 and 2.

Cantilever shear wall

The geometry, loadings and reinforcement configuration of the studied shear wall are illustrated in Figure 9. A single spread–of–plasticity element, fully supported at its base, is employed to idealize this structural component. Tests were also performed where more spread–of–plasticity elements were used. The results were identical (difference in total displacements less than 1%) when compared with a single element which used ten Gaussian points of integration over the element length. The bilinear stress–strain relation

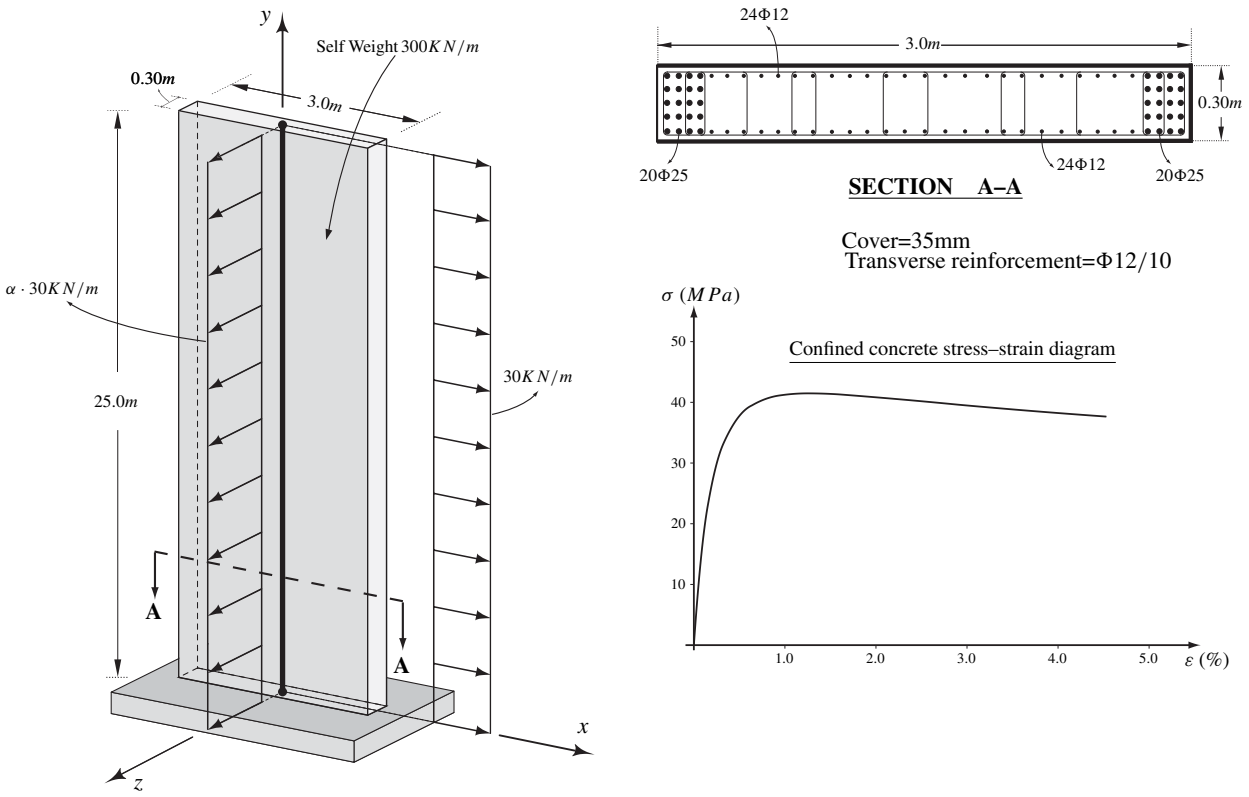

Figure 9: Cantilever shear wall.

for reinforcing steel and Mander's model for confined concrete (Figure 9) that were used in the previous example, are employed again here. In this case, the ultimate compressive strain of confined concrete is 4.53%. A constant vertical loading and an incremental lateral loading in the major direction of the shear wall are applied.

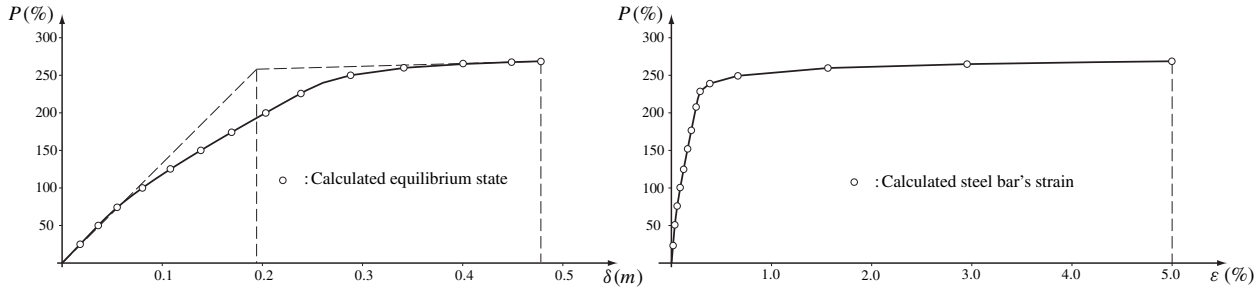

Figure 10: Lateral load–top displacement curve of R/C wall and lateral load–strain curve for the most tensiled steel bar.

The lateral load–top displacement curve for this wall is illustrated in Figure 10. From this figure the ductility capacity of the wall is calculated:

$$\mu = \frac{\delta_{max}}{\delta_y} = \frac{0.478}{0.193} = 2.48$$

Finally, the lateral load–strain curves for the steel bars that exhibit the highest tensile strain at the lower end–section of the wall are also shown in Figure 10.

Biaxial lateral loading

The cantilever shear wall (Figure 9) previously analyzed, is again employed here to perform a series of pushover analyses where the lateral loads used are: (a) in the major direction of the shear wall $30KN/m$ uniform load and (b) in the minor direction a percentage (α) of the previous load. The lateral load–top displacement (in the major direction) curves are illustrated in Figure 11. The gradual decrease in the slope of each curve is due to the existence of multiple layers of reinforcement steel bars that do not yield simultaneously.

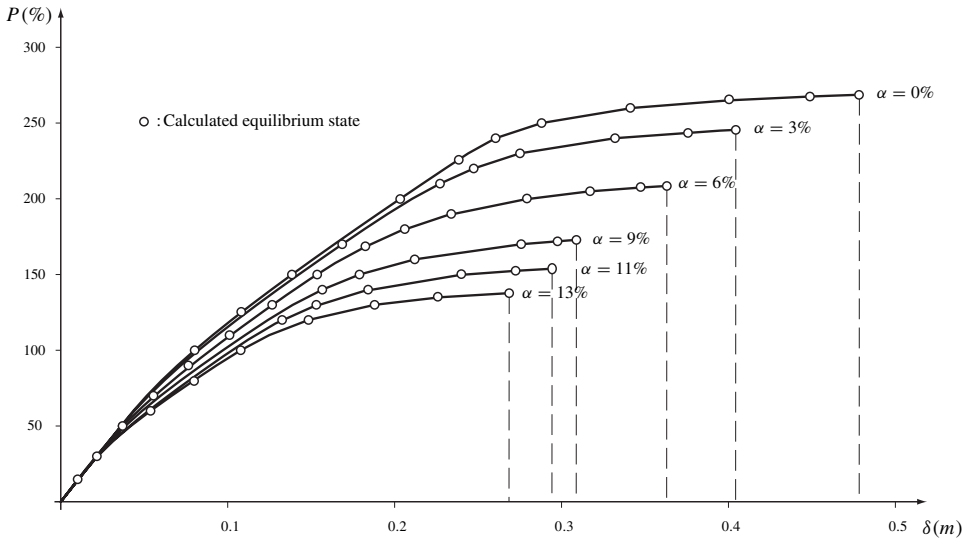

Figure 11: Lateral load–top displacement curves for various factors (α) of the lateral load in the minor direction of the shear wall.

Table 3: Analysis results of the cantilever shear wall under biaxial lateral loading

Load Factor $\alpha(\%)$	δ_y (mm)	δ_{max} (mm)	Ductility	Reduction in δ_{max} (%)
0	193	478	2.48	–
3	177	404	2.28	15.5
6	150	363	2.42	24.0
9	124	309	2.49	35.5
11	110	294	2.67	38.5
13	99	268	2.70	43.9

The ductility capacities calculated for each analysis are summarized in table 3. It is safe to conclude based on the above, that as the lateral load intensity in the minor direction increases, the top displacement in the

major direction is reduced, even though the ductility ratios remain approximately the same. It should be noted that even a small percentage of the above loading results in a significant reduction of the total inelastic base rotation capacity of the shear wall.

CONCLUSIONS

This paper presents a new spread–of–plasticity analysis procedure that is implemented in the case of R/C space frame buildings. An efficient beam/column element is introduced, which can take into account the spreading of plasticity along the element's length. The new element formulation makes no assumption of the deformed shape of the element, as it does not utilize any shape functions. On the contrary, it takes into account the real (non–linear) deformations of the cross–sections under the applied normal stress resultants ($R_{x'}$, $M_{y'}$, $M_{z'}$). Therefore, this approach does not require a discretization of each physical member into a number of elements in order to achieve adequate accuracy of the obtained results.
This new spread–of–plasticity analysis procedure is used for the non–linear static analysis of two R/C structures: an eight–storey frame and a cantilever shear wall. For both structures the global ductility capacity is estimated and local ductility capacities, expressed in terms of lateral load–strain curves of specific steel bars, are also presented. Finally, the shear wall is subjected to biaxial lateral loading. In that event, it is noticed that the existence of lateral loading in the minor direction of the wall leads to a significant reduction of the total rotation capacity at its base.

REFERENCES

1. SAP2000, "Detailed Tutorial Including Pushover Analysis", Berkeley, California.
2. GTSTRUDL, "Analysis User's Guide", Atlanta, Georgia.
3. Kim K., Engelhardt M., "Beam-column element for nonlinear seismic analysis of steel frames" Journal of Structural Engineering 2000; 126(8): 916-925.
4. ANSYS, "Ansys Theory Reference".
5. ADINA, "Theory and Modeling Guide", Volume 1.
6. Davenne L., Ragueneau F., Mazars J., Ibrahimbegovic A. "Efficient aproaches to finite element analysis in eathquake engineering", Computers and Structures 2003; 81: 1223-1239.
7. Przemieniecky JS., "Theory of matrix structural analysis" New-York: MCGraw-Hill, 1985
8. Izzuddin BA., Siyam AAFM., Lloyd Smith D., "An efficient beam-column formulation for 3D reinforced concrete frames", Computers and Structures 2002; 80: 659-676.
9. Ikonomou A., "Statics of structures" University Lectures Handbook 1998, Volume 2, Patras, Greece.
10. Marathias P.,"Statics of structures - Analysis of linear structures", University Lectures Handbook 2002, Patras, Greece.
11. Konrad A., "Ermittlung des Dehnungszustands beliebiger Stahlbetonquerschnitte mit dem Newton-Verfahren", Beton-und Stahlbetonbau 1988; 83(10): 261-264.
12. Mander J.B., Priestley M.J.N., and Park R., "Observed Stress-Strain Behaviour of Confined Concrete", Journal of the Structural Division, ASCE 1977; 103(10): 1953-1970.